11

Arterial Plaque Characterization Using IVUS Radio-Frequency Time Echoes

Rafik Borji and Matthew A. Franchek
University of Houston, Department of Mechanical Engineering
USA

1. Introduction

The reported yearly worldwide death tolls and especially in the US about cardio-vascular disease is the leading factor that motivated scientists to invest time and money in order to find innovative ways that enable accurate and early detection of such diseases (American Heart Association [AHA], 2006; AHA, 2008). Since CVD occurs within the human body, imaging modalities were invented to present a picture of the artery as close as possible to its real status. These imaging methods accompanied with continuous developments have helped tremendously in the improvement of proactive health care and early interventions before aggravations. Intravascular Ultrasound (IVUS) is one of the cost effective modalities that have been extensively used for diagnostics purposes (Gaster et al., 2003; Mueller et al., 2003). Although IVUS has the advantage of differentiating between all the artery cross-section components in terms of geometry (Nissen & Yock, 2001), the composition and mechanical properties of each component is still a subject of discussion and research. In fact, an objective classification of plaques based on both mechanical and acoustic properties is not reached yet. For instance, echogenicity of luminal tissue in most cases is the same for a plaque composed of high lipid depositions (Stary, 1992; Stary et al., 1994; Stary et al., 1995). Thus ultrasound wave propagation and transmission should be studied fundamentally in the human tissues and specifically through the artery cross-sections. The only way these ultrasonic waves could be studied meticulously is by solving the propagation governing equations, i.e., through the wave equation. Finding the analytical solution of these waves contributes definitely in understanding the propagation fashion and behavior inside the medium. Finding analytical solution of the wave equation is highly dependent on the medium. In the case of artery cross-section in a human body, there exist numerous geometric irregularities. These irregular shaped components of the artery make the wave equation unsolvable analytically. Consequently numerical methods are employed to find discrete solutions of the ultrasound waves.

The inability of discriminating most plaque types from the grayscale images has fostered researchers to think about the content and information that the IVUS backscattered radio-frequency (RF) ultrasound waves could offer. Studies have shown that RF signals possess valuable information in terms of plaque composition (Normal, fatty, fibro-fatty, fibrous, fibrous with calcification). It has been noticed that there is a difference between these RF echoes coming from various plaque types (Urbani et al., 1993).

Integrated backscatter IVUS (IB IVUS) was introduced and calculated based on these RF signals. Despite the accurate differentiation between all plaque types (calcification, mixed lesion, fibrous tissue, lipid core and thrombus) using IB IVUS, the angle dependency between ROI's and catheter axis makes this classification unstable and sensitive (Urbani et al., 1993; Picano et al., 1983; Sarnelli et al.,1986; Landini et al., 1986; Barzilai et al., 1987; De Kroon et al., 1991; Picano et al., 1994). Moreover the high resolution dictated for plaque detection necessitates high frequency ultrasound signals which affect the penetration depth of these transmitted ultrasonic pulses.

In addition to the use of IB as a determinant parameter by which plaques were classified, new research directions has been inspired from the elastic property that could characterize each plaque type. This gave rise to what is called **intravascular elastography** (also known as **IVUS elastography**) (Cespedes et al., 1991). In fact, investigators have taken advantage of the possibility of recording the RF echoes to use them for displacements or strain determination (Ryan & Foster, 1997; De Korte et al., 1998; Schaar et al., 2003; Saijo et al., 2004; Shapo et al., 1996). Despite the striking difference of the strain values for various plaques, most of the studies were performed in vitro where the temperature is different from in vivo case. Additionally excised arteries were used after freezing and thawing which influences the values of elastic modulus. Elastography has also been criticized for its inability of discriminating between normal artery and Fibrous caps (De Korte et al., 2000).

The use of the RF echoes content has also been used further. A method called **virtual histology** (also called **VH IVUS**) based on these IVUS-RF-ultrasonic waves has been developed. This tissue characterization technique is based on the frequency spectrum analysis (Koenig & Klauss, 2007; Nair et al., 2002). Several limitations accompanied the development of VH IVUS. In fact, virtual histology gives an axial resolution which is too low to detect fibrous cap thickness. In addition the detection between soft plaque material and thrombus is not possible.

Despite this simplicity of image construction from IVUS and the development of some signal processing procedures to overcome the lack of plaque characterization, there are significant challenges which limited the accuracy and clarity of the images produced via IVUS. These challenges are always present in the imaging process. For example, the omnipresence of noise related to the acquisition of the ultrasound waves (due to electronic devices) plays an important role on hiding useful information during the detection process. Moreover uncertainties due to sound speed variation, eccentricity of the transducer as well as scattering (related to small particles such as cells, and irregular surfaces) are important factors which contribute to the limitations of the developed IVUS techniques for the identification of vulnerable plaques. This certainly influences the issues of resolution and inability to adequately discriminate between fibrous and lipid-rich plaques.

The nature of this imaging modality (irregularities in the geometry of the tissues and movement of the catheter tips) and the sensitivity of the recorded RF echoes have motivated other research groups to work on modeling the ultrasound wave propagation in biological tissues and specifically IVUS.

Since the IVUS imaging method is based on ultrasound wave propagation, the only way to sketch a model for this propagation will be dictated from the constitutive laws that govern these waves. To know the complete behavior of the waves towards each tissue component, a solution should be found in time and space for these signals.

Nonlinear propagation mathematical models have been introduced. The most widely used model for modeling finite amplitude sound beam propagation is the so-called Khokhlov, Zabolotskaya and Kuznetsov (KZK) equation (Kuznestov, 1971). Numerous methods to solve this non-linear model have been proposed (Lee & Hamilton, 1995; Tavakkoli et al., 1998). One of the difficulties for these numerical models was the computational aspect. Huge memory and supercomputing machines have to be allocated for the implementation of such nonlinear models. Even using advanced equipments in terms of performance, the computation process of these models can take several hours and even days. This is far from simulating a real time propagation of the ultrasonic waves.

Given the complexity in solving these nonlinear models, other groups of researchers have resorted to the adoption of simple linear wave equation models (Kendall & Weimin, 2001). In fact ultrasound that is propagating in biological tissues generates small fluctuations. The propagation of these fluctuations is governed by what is called the wave equation. The closed form solution of the wave equation here above is unavailable. Thus two main numerical methods were proposed; which are the finite differences and the finite element methods (Guenther & John, 1996; Kendall & Weimin, 2001). The complexity of the models presented problems in terms of real time simulation and computational burden.

A reduced order model called Transmission Line matrix (TLM) method is developed in this chapter to simulate the ultrasound wave propagation. The foundation of the computational method (Transmission Line Matrix Method) that is used to model IVUS in a simple regular medium (rectangular shape) is first developed. A new TLM model in polar coordinates (circular shape to model the artery cross-section) is then outlined. The TLM model will subsequently be modified to model IVUS. The system identification methodology used to construct a parametric model that characterizes a plaque for specific mechanical and acoustic properties is demonstrated in the last part of the chapter.

2. TLM model

Transmission Line Matrix concept was based on transmission lines (Fig. 1).

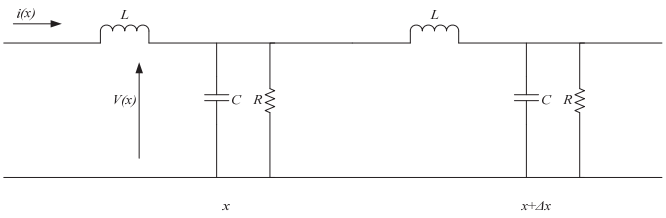

Fig. 1. A simple transmission line circuit between points x and x+Δx

The idea of using electrical circuits for TLM came from the analogy that was established between the current or voltage propagating in this line from one point to another and the electromagnetic field (EMF) governing equations (Christos, 1995). Besides this analogy, TLM was based on the Huygens principle where each point of a wave front is regarded as a secondary wave source point and the surface tangent to the secondary wave fronts is used to determine the future position of wave front (Fig. 2).

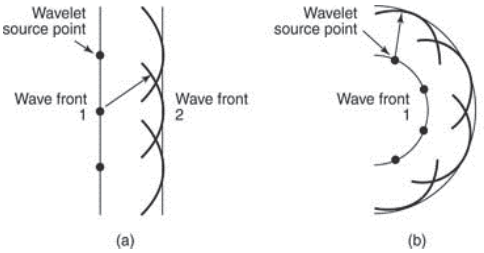

Fig. 2. Schematics of the Huygens principle for wave propagation (CliffsNotes. Wave Optics, 2010)

TLM models this physics principle by discretizing the medium into a mesh grid and replacing the wave amplitudes by voltages and currents traveling from one node to another (Fig. 3).

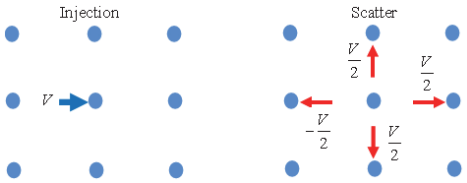

Fig. 3. Propagation in TLM model

2.1 Rectangular TLM

The 2-D TLM method has been widely developed and studied in the literature because of its importance in terms of treating wave propagation in the two dimensional space (Christos, 1995; De Cogan et al., 2006). As mentioned previously the use of TLM method for wave propagation purposes was first inspired from the analogy that was found between the electric circuit variables and the EMF problem. A two dimensional element of a medium of dimensions u and v, is represented by a node intersected by two transmission lines in the x and y directions (Fig. 4).

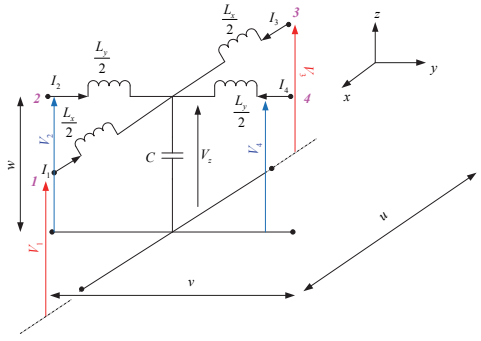

Fig. 4. Shunt TLM node

If C is the total capacitance of this element and L_x, L_y are the total inductances for the two lines in x and y directions respectively, then the voltage/current differential equations are

$$\begin{cases} \dfrac{\partial V_z}{\partial x} = -\dfrac{L_x}{u}\dfrac{\partial I_x}{\partial t} \\ \dfrac{\partial V_z}{\partial y} = -\dfrac{L_y}{v}\dfrac{\partial I_y}{\partial t} \\ -u\dfrac{\partial I_x}{\partial x} - v\dfrac{\partial I_y}{\partial y} = C\dfrac{\partial V_z}{\partial t} \end{cases}, \tag{1}$$

where I_x and I_y are the current traveling in the lines in x and y directions respectively and V_z is the total voltage in the element. Recall that the governing equations for EMF and Sound wave problems in the 2-D configuration are the following.

$$\begin{cases} \dfrac{\partial E_z}{\partial x} = \mu\dfrac{\partial H_y}{\partial t} \\ \dfrac{\partial E_z}{\partial y} = -\mu\dfrac{\partial H_x}{\partial t} \\ \dfrac{\partial H_y}{\partial x} - \dfrac{\partial Hx}{\partial y} = \varepsilon\dfrac{\partial E_z}{\partial t} \end{cases}. \tag{2}$$

$$\begin{cases} \dfrac{\partial P}{\partial x} = -\rho\dfrac{\partial U_x}{\partial t} \\ \dfrac{\partial P}{\partial y} = -\rho\dfrac{\partial U_y}{\partial t} \\ -\dfrac{\partial U_x}{\partial x} - \dfrac{\partial U_y}{\partial y} = \sigma\dfrac{\partial P}{\partial t} \end{cases}. \tag{3}$$

Where E and H are the Electric and magnetic fields, μ and ε are the permeability and permittivity of the space. P is the pressure, U_x and U_y are the pressure velocity components in x and y directions, ρ is the density of the medium and σ is the compressibility of the medium.

The system of equations in (1) is transformed to equation (4)

$$\begin{cases} \dfrac{\partial\left(\dfrac{V_z}{w}\right)}{\partial x} = \dfrac{L_x v}{uw}\dfrac{\partial\left(-\dfrac{I_x}{v}\right)}{\partial t} \\ \dfrac{\partial\left(\dfrac{V_z}{w}\right)}{\partial y} = -\dfrac{L_y u}{vw}\dfrac{\partial\left(\dfrac{I_y}{u}\right)}{\partial t} \\ \dfrac{\partial\left(-\dfrac{I_x}{v}\right)}{\partial x} - \dfrac{\partial\left(\dfrac{I_y}{u}\right)}{\partial y} = \dfrac{Cw}{uv}\dfrac{\partial\left(\dfrac{V_z}{w}\right)}{\partial t} \end{cases}. \tag{4}$$

Here w is an arbitrary distance inserted to retain the correct dimensionality when dividing I_x and I_y by v and u respectively (Al-Mukhtar & Sitch, 1981). Comparing equations (2), (3) and (4), the analogy between EMF, sound propagation and electric circuits is established in Table 1. From this analogy the electric and magnetic fields of the EMF problem could be solved through the TLM method by considering them as the transmission line voltage and currents respectively. The same thing applies for the sound wave problem (wave equation), where the amplitudes are calculated via the voltages traveling in the TLM model.

EMF parameters	Sound wave parameters	Electric Circuit Parameters for the Transmission Line (TL)
E_z	P	V_z/w
$-H_y$	U_x	I_x/v
H_x	U_y	I_y/u
μ	ρ	$L_y u/vw$ or $L_x v/uw$
ε	σ	Cw/uv

Table 1. Analogy between EMF, Sound wave and TL parameters

In a regular mesh, each node is characterized by equally spaced nodes related to each other by four lines (in the x and y directions) as illustrated in Fig. 4. This shunt node in a Cartesian regular mesh is presented by four transmission line segments each of characteristic impedance $Z_i, i = 1,2,3,4$. These four lines have the same length (i.e. same impedance). The scattering is calculated based on the incident $\left({}_kV_i^I\right)$ and reflected $\left({}_kV_i^R\right)$ pulses to the node and the relationship between them. This relationship between $\left({}_kV_i^I\right)$ and $\left({}_kV_i^R\right)$ is derived using a general approach based on replacing each of the line segment by its Thevenin equivalent (U.A. Bakshi & V.U. Bakshi, 2009). For each segment, this consists of a voltage $2{}_kV_i^I$ in series with the impedance Z_i (Fig. 5).

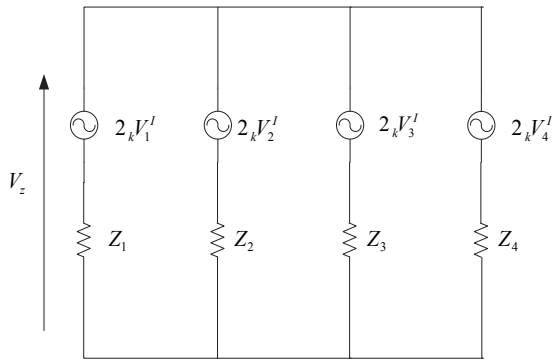

Fig. 5. Thevenin equivalent circuit for the 4 lines intersecting the shunt node of the mesh

The scattering matrix for the shunt node

$$\begin{bmatrix} {}_kV_1^R \\ {}_kV_2^R \\ {}_kV_3^R \\ {}_kV_4^R \end{bmatrix} = 0.5 \begin{bmatrix} -1 & 1 & 1 & 1 \\ 1 & -1 & 1 & 1 \\ 1 & 1 & -1 & 1 \\ 1 & 1 & 1 & -1 \end{bmatrix} \begin{bmatrix} {}_kV_1^I \\ {}_kV_2^I \\ {}_kV_3^I \\ {}_kV_4^I \end{bmatrix}. \tag{5}$$

There are applications, such as arteries, when the medium geometry is complex (curved or circular shapes), where the use of the regular TLM method is not appropriate to solve numerically the sound wave equation. This restriction on the shape and size of the mesh affects the capability of the conventional regular TLM method. Moreover the employment of the conventional TLM where the shape is irregular necessitates the use of finer meshes to represent these irregularities accurately. This represents a burden in terms of memory use and run time for numerical computations. Hence a new TLM mesh and model will be developed for the whole artery cross-section in the next section.

2.2 Cylindrical TLM

A two dimensional element of a medium having differing dimensions u and v, is represented by a node intersected by two transmission lines in x and y directions (Fig. 6).

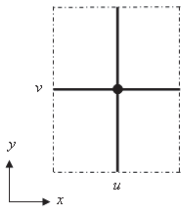

Fig. 6. Irregularly spaced element

From Table 1, the following relationships are obtained

$$\begin{cases} C = \sigma \dfrac{uv}{w} \\ L_x = \rho \dfrac{uw}{v} \\ L_y = \rho \dfrac{vw}{u} \end{cases}. \tag{6}$$

Time synchronism is conserved in the TLM (Christos, 1995). In fact, the transmitted pulse from one node must reach its surrounding nodes at the same time regardless the lines lengths linking these nodes in all direction (x and y directions in the 2-D case). This means that the velocity of propagation of the voltage is dependent on the lines lengths. Since the velocity is function of the total inductance and capacitance of the line ($V = \dfrac{1}{\sqrt{LC}}$), the inductance term is fixed and capacitance is calculated for each direction by taking into account the relationship between inductance, capacitance and velocity.

Given the inductances in both directions, the capacitances per unit length in these lines are obtained.

$$\begin{cases} C_x = \dfrac{\sigma_0 v}{u^2 h \rho_r w} \\ C_y = \dfrac{\sigma_0 u}{v^2 h \rho_r w} \end{cases}. \tag{7}$$

Due to the irregular mesh grid, the total capacitances found in x and y directions, C_x and C_y are sometimes less than the total capacitance of the element C. A residual capacitance C_s is defined and modeled by an open-circuit stub at each node of the mesh (Fig. 7).

$$C_s = \sigma \frac{uv}{w} - \frac{\sigma_0 \left(u^2 + v^2\right)}{uvh\rho_r w} \tag{8}$$

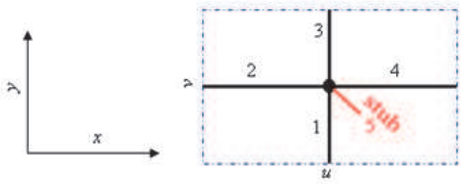

Fig. 7. Stub represented by a new line at each node

The artery cross-section is presented by a disk. The coordinates system is characterized by the angle θ and the radial position r (polar coordinates). In the TLM method, the discretization process of the medium will lead to an irregular gridding (Fig. 8).

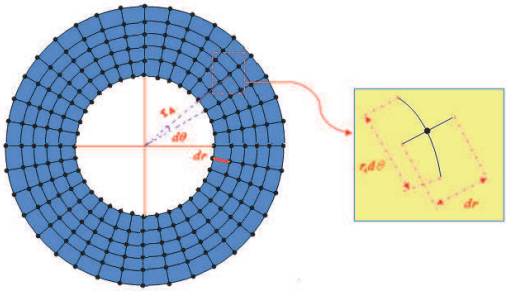

Fig. 8. Irregular structure of a circular element of the cylindrical TLM model

In general for an arbitrary node that has a radial position r the element is characterized by the following lines lengths

$$\begin{cases} u_r = dr \\ u_\theta = rd\theta \end{cases} \tag{9}$$

Obviously the nodes in this case are not equally spaced. Therefore the TLM model corresponds exactly to the same formulation. Consequently a stub line must be added to compensate for the residual capacitance caused by the length difference of the radial and angular lines of each element in the mesh. The element is characterized by radial and angular impedances and a stub admittance Z_r , Z_θ and Z_5 .

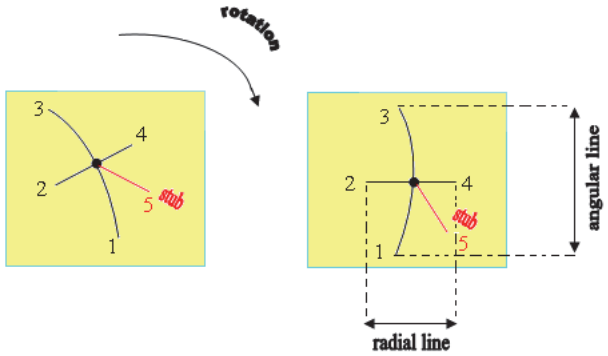

Fig. 9. Added stub line to a circular element

In Fig. 9, the radial line $[2,4]$, the angular line $[1,3]$ and the stub line are characterized respectively by Z_r , Z_θ and Z_5 .The radial, angular impedances and the stub admittance can be derived by replacing u by dr and v by $rd\theta$.

$$\begin{cases} Z_r = \dfrac{w dr \rho_r}{r d\theta} Z_{ref} \\ Z_\theta = \dfrac{w r d\theta \rho_r}{dr} Z_{ref} \\ Z_5 = \dfrac{2\left[\sigma (dr)^2 (rd\theta)^2 h\rho_r - \sigma_0 \left((dr)^2 + (rd\theta)^2\right)\right]}{(dr)(rd\theta) w \sigma_0 \rho_r} \end{cases}, \tag{10}$$

where $\rho_r = \dfrac{\rho}{\rho_0}$ is the ratio of a line inductance with respect to the smallest line inductance and $Z_{ref} = \sqrt{\dfrac{h\rho_0}{\sigma_0}}$ is the characteristic impedance of the smallest line in the mesh grid of the artery cross-section. ρ_0 and $\dfrac{\sigma_0}{h}$ are the inductance and capacitance of the reference line (i.e. smallest line).

For both Cartesian and cylindrical geometry, each TLM element is thus characterized by a circuit structure of five transmission lines (Fig. 10).

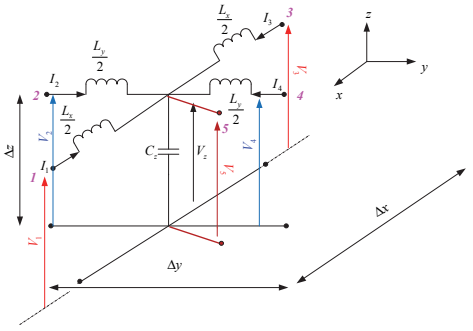

Fig. 10. Shunt node for irregular TLM

The equivalent Thevenin circuit is composed of five Thevenin sources in series with five equivalent impedances corresponding to the five lines (Fig. 11).

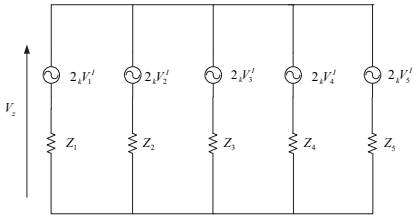

Fig. 11. Thevenin equivalent circuit for the 5 lines intersecting an arbitrary node of the irregular mesh

The scattering matrix equation in this case is

$$\begin{bmatrix} {}_kV_1^R \\ {}_kV_2^R \\ {}_kV_3^R \\ {}_kV_4^R \\ {}_kV_5^R \end{bmatrix} = \frac{1}{D}\begin{bmatrix} 2Z_1 - D & 2Z_2 & 2Z_3 & 2Z_4 & 2Z_5 \\ 2Z_1 & 2Z_2 - D & 2Z_3 & 2Z_4 & 2Z_5 \\ 2Z_1 & 2Z_2 & 2Z_3 - D & 2Z_4 & 2Z_5 \\ 2Z_1 & 2Z_2 & 2Z_3 & 2Z_4 - D & 2Z_5 \\ 2Z_1 & 2Z_2 & 2Z_3 & 2Z_4 & 2Z_5 - D \end{bmatrix}\begin{bmatrix} {}_kV_1^I \\ {}_kV_2^I \\ {}_kV_3^I \\ {}_kV_4^I \\ {}_kV_5^I \end{bmatrix}. \quad (11)$$

${}_kV_i^R$ and ${}_kV_i^I$ are the reflected and incident voltages to an arbitrary node of the line i at time k and $D = \sum_{i=1}^{5} Z_i$ is the sum of the impedances of the four lines and the stub admittance.

3. TLM IVUS model

Ultrasound waves have the same properties as sound waves. They obey the same wave propagation law. In this section a physics-based numerical model is developed using TLM method to mimic the ultrasound wave propagation inside the arterial wall. Both rectangular and cylindrical TLM models will be employed to model IVUS. The first TLM model is used

by considering a small portion of the artery cross-section that has a rectangular shape (Fig. 14). However the second TLM model (cylindrical) takes into account the whole artery cross-section geometry. These codes were developed in Matlab. In order to construct the TLM models many basic parameters should be provided. The size of the medium, the gridding rate, the boundary termination, the wave source location and the traveling process are the most important data to be known in the modeling process.

The medium is automatically generated from the developed TLM codes once the dimensions are specified. Given the inner and outer radii of the artery cross-section, an automated mesh is generated. Since TLM model is based on the nodes and lines of the discretized medium, the number of nodes in both directions as well as the lines lengths are function of the indicated gridding rates. In the cylindrical TLM model, the choice of the gridding rate is essential for capturing the propagation of the ultrasound wave. The wave should reach the outer edge of the artery cross-section. In fact for an arbitrary mesh the propagation trend of the ultrasound wave is more pronounced in the angular direction of the circular medium. The choice of the mesh grid must be generated in a way that guarantees a conic wave propagation of the TLM method. This means that the propagation should occur in a conic way in the radial direction. The propagation as developed previously in the TLM model depends on the scattering matrix which is function of the lines impedances. These impedances are function of the gridding rates in both radial and angular directions. Thus a specific mesh grid should be developed to ensure this numerical stability. The propagation of the sound wave is expected to be like the one illustrated by Fig. 12.

Investigations have shown that the angular deviation of the propagation occurs when the radial position is characterized by $\frac{Z_r}{Z_\theta} = 0.633$. Since $\frac{Z_r}{Z_\theta} = \frac{(dr)^2}{(Rd\theta)^2}$, after this radial position, the ratio between the gridding rates has this condition $\frac{dr}{Rd\theta} < 0.8$. The mesh grid is designed such that $\frac{dr}{Rd\theta} \geq 0.8$. By imposing this numerical condition on the mesh grid, the propagation occurs in a conic fashion as illustrated in Fig. 12.

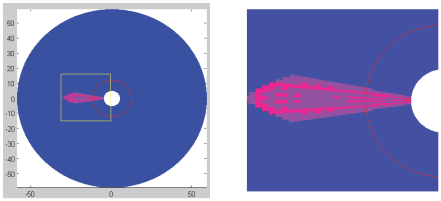

Fig. 12. Conic propagation of the sent wave through the circular medium

As the TLM is a numerical method, the medium should be of a finite size. This is known as **medium termination**. This is presented by a wall that is characterized by the same acoustic impedance of the terminated medium. For example if the external medium that comes after the artery is air, then the wall that models the termination of air is characterized by the acoustic impedance of the air. For all the developed simulations the surrounding media impedances will be taken in such a way the boundary reflection effect is attenuated so that these reflected components do not influence the wave propagation inside the artery cross-section.

The design of **the wave source** has been widely studied for the IVUS. In the TLM model, flexibility is given in the code to design any kind of source waves. Since Matlab is the platform where the code was developed, SIMULINK toolbox is used for the source wave specifications. This toolbox offers a variety of signals some of them are illustrated in Fig. 13. In addition to the wide range of source waves, this model gives the possibility of specifying any location in the mesh to be the source point where the ultrasonic wave starts to propagate. For instance the source could be in one node of the edges of the medium, inside the medium or in different nodes at the same time.

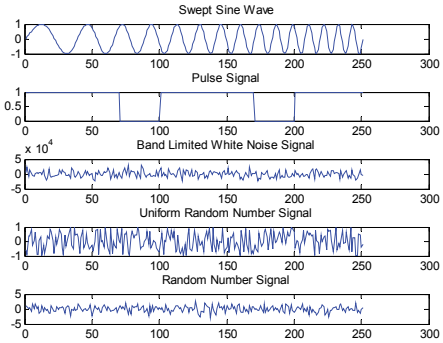

Fig. 13. Examples of different source waves designed by Simulink

The propagation process is based in the Huygens principle where for a given node in the mesh, the reflected amplitudes going out at time k will serve as the incident waves to the surrounding nodes at time $k+1$. For the rectangular and cylindrical TLM models, it is given by equations (12) and (13).

$$\begin{cases} {}_{k}V_1^R(x_0,y_0) = {}_{k+1}V_3^I(x_0,y_0-\Delta y) \\ {}_{k}V_2^R(x_0,y_0) = {}_{k+1}V_4^I(x_0-\Delta x,y_0) \\ {}_{k}V_3^R(x_0,y_0) = {}_{k+1}V_1^I(x_0,y_0+\Delta y) \\ {}_{k}V_4^R(x_0,y_0) = {}_{k+1}V_2^I(x_0+\Delta x,y_0) \end{cases} \tag{12}$$

$$\begin{cases} {}_{k+1}V_1^I(r_0,\theta_0+d\theta) = {}_{k}V_3^R(r_0,\theta_0) \\ {}_{k+1}V_2^I(r_0+dr,\theta_0) = {}_{k}V_4^R(r_0,\theta_0) \\ {}_{k+1}V_3^I(r_0,\theta_0-d\theta) = {}_{k}V_1^R(r_0,\theta_0) \\ {}_{k+1}V_4^I(r_0-dr,\theta_0) = {}_{k}V_2^R(r_0,\theta_0) \\ {}_{k+1}V_5^I(r_0,\theta_0) = {}_{k}V_5^R(r_0,\theta_0) \end{cases} \tag{13}$$

The IVUS TLM models can represent both healthy and abnormal artery cross-sections. In the healthy case the TLM model is described by a medium that has constant acoustic impedance ($Z = \rho c$, ρ is the medium density and c is the acoustic speed in the medium). However the abnormal artery is modeled by an inclusion that is inserted in the healthy medium. This inclusion is characterized ban acoustic impedance that is different from the one of the healthy medium. Illustrated in Fig. 14 is the case where artery contains a plaque (Yellow colored region).

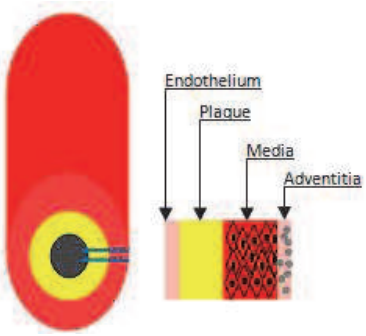

Fig. 14. Plaque in the artery

The TLM model will consider the plaque as a rectangular object that is inserted inside the artery portion presented by the rectangular medium. The plaque (inclusion) that is formed inside the artery is characterized by different acoustic properties. In fact the ultrasound speed and density are not the same as of the normal tissue (i.e. different acoustic impedances). This will produce a boundary between the healthy portion of the artery and the abnormality edge. This boundary characterizes a change in impedances. A reflection/transmission phenomenon takes place due to this change along the four edges of the plaque. Considering $Z_{Plaque} = c_{Plaque}\rho_{PLaque}$ and $Z_{Artery} = c_{artery}\rho_{Artery}$ to be the acoustic impedances of the plaque and artery, then the reflection and transmission coefficients are

$$R = \frac{Z_{Plaque} - Z_{Artery}}{Z_{Plaque} + Z_{Artery}}$$
$$T = 1 - \frac{Z_{Plaque} - Z_{Artery}}{Z_{Plaque} + Z_{Artery}} \quad . \tag{14}$$

The transmission and reflection that occur on both sides of the boundary are function of these coefficients. Depending on the acoustic characteristics of the plaque the propagation of the wave will show different behavior. As an example to illustrate the effect of the plaque, three different acoustic impedances are taken. A swept sine wave is designed to be the source signal at the node (1st horizontal, 45th vertical). The medium is composed of 751 by 76 nodes and the plaque is located between the 20th and 30th node in the horizontal direction and the 25th and 65th node in the vertical direction (Fig. 15).

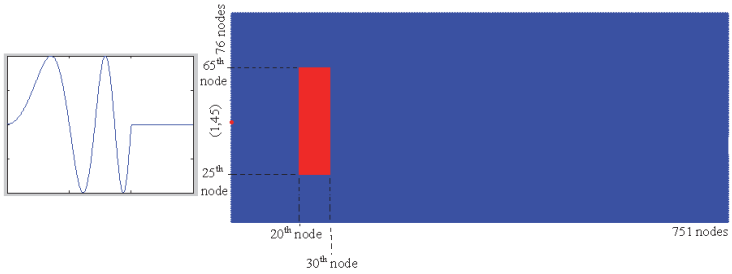

Fig. 15. Plaque example generated by the developed 2-D rectangular TLM model

Fig. 16 is an illustration of the plaque influence on the determination of the wave shape using regular TLM model. This model could be extended to study numerous cases where all combinations of abnormalities can be constructed.

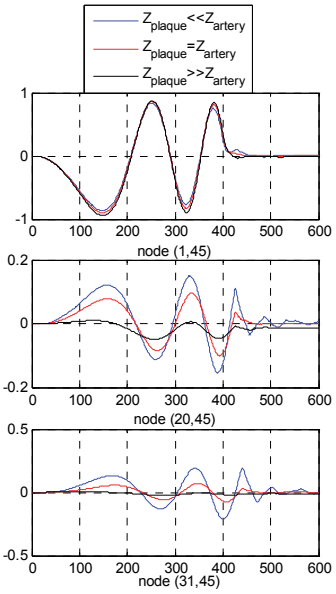

Fig. 16. Comparison of the time signals using the rectangular TLM model ($Z_{Hardinclusion} = 7.4Z_{Healthyartery}$ and $Z_{Softinclusion} = 0.074Z_{Healthyartery}$)

Also using the cylindrical TLM model, an inclusion was inserted in the circular medium between the 70th and 130th angular nodes and 20th and 30th radial nodes. A sine wave is injected from the inner radius (node (1st radial direction, 100th angular direction)) and the wave propagation is recorded. It can be shown from Fig. 17, the effect of the acoustic properties of the inclusions that form inside the artery. These models will be employed in the next section to analyze these recorded signals and build a lumped parameter model of the different tissues types based on their size and acoustic properties.

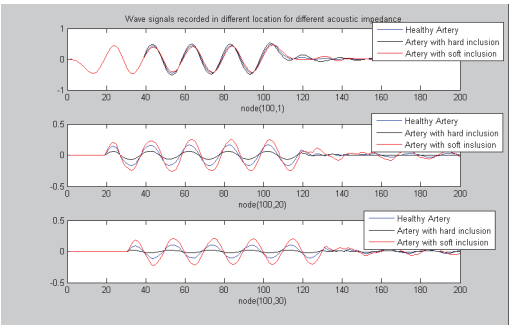

Fig. 17. Time signals record of the wave propagation at different locations having different inclusion ($Z_{Hardinclsuion} = 7.4Z_{\text{healthy artery}}$ and $Z_{Softinclsuion} = 0.074Z_{\text{healthy artery}}$)

4. Plaque characterization

This section departs from the traditional approaches appearing in the literature by considering the inclusion within a medium to be a dynamic system. A system identification approach will be adopted to characterize the dynamics of the plaque (Soderstrom & Stoica, 2001). Thus, the TLM models developed in the previous sections are used as a mean of acquiring the time signals transmitted and reflected in a region of interest within the medium (plaque or inclusion location). These signals will be considered as inputs and outputs to the dynamic system where digital signal processing techniques are employed to identify a parametric model for these plaques.

4.1 Persistency of excitation of the input signal

Any input signal used in the context of system identification must meet certain condition. In particular, the input signal should be **persistently exciting** (Ljung, 1999). The frequency domain condition enforcing a persistency of excitation is:

A signal $u(t)$ *characterized by its spectrum* $\Phi_u(\omega)$ *is said to be persistently exciting if*

$$\Phi_u(\omega) > 0 \qquad \text{for almost all } \omega$$

Thus the spectrum may be zero on a set of number of points (almost all definition).

One classical frequency-rich signal is the swept sine signal which is also known as the "chirp signal". The chirp signal is a single sine wave with a frequency that is changing continuously as a function of time. The general mathematical presentation of the swept sine wave is

$$u(k) = A\sin\left(2\pi\beta(k) * \frac{(k-1)}{f_s} + \varphi\right) + B$$

$$\beta(k) = f_{\min} + \frac{(f_{\max} - f_{\min})}{2t_{\arg et}}\left(\frac{k-1}{f_s}\right) \quad \text{where } f_s \geq 2f_{\max}$$

Where A is the wave amplitude, B is the signal bias term, φ is the phase angle of the wave and $\beta(k)$ is the time varying frequency of the swept sine in Hertz. The frequency f_s is the sampling frequency. The frequency $\beta(k)$ in this case is a linearly varying frequency over the interval $[f_{\min}, f_{\max}]$. The target time, denoted as t_{target}, is the time for which the upper bound of the frequency range is achieved. During the system identification process of the plaque and healthy tissue characterization, a swept sine will be designed as the source signal (the choice of the swept sign came from the fact that this wave was the only signal that was consistent in terms of constancy of the model structure). From literature, the frequency range used in the signal processing for the soft tissue is in the range of $[10^5, 10^7] Hz$. The swept sine is therefore designed such that the frequency covers this range. This signal will be combined with a zero-element vector. As illustrated in Fig. 18, a swept sine is designed to be the source signal of the simulation part for the TLM models. The sampling time of this signal is equal to 10^{-9} sec.

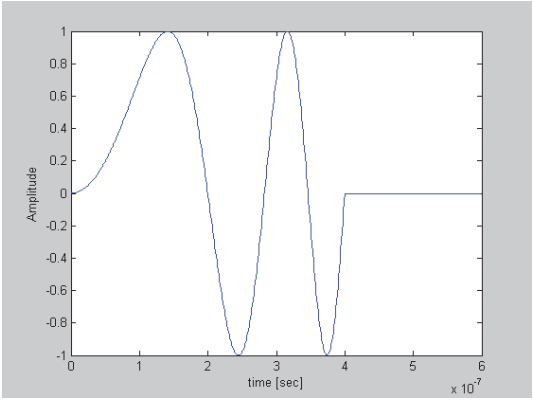

Fig. 18. Constructed swept sine pulse

4.2 System identification method

This process is composed of two stages. In the first stage, the identification technique that is used for modeling purposes is the so-called *Orthogonal Least Squares* (OLS) method (Korenberg et al., 1988; Chen et al., 1989). This method is a discrete time domain based approach where the time signals are used for model determination. In fact, the transient time domain information generated from the TLM artery models and their delayed components will be used as possible input regressors. This method will determine the most significant regressors from a broad range of possible candidates to identify the best parametric model. The general model structure can be linear or nonlinear. However for this work, it is anticipated that only a linear model will be needed.

A discrete time model generally resembles a polynomial structure. Considering a general case, a discrete system model with unknown coefficients (model parameters to be estimate) can be transformed into the linear-in-the-parameters representation by means of the expansion

$$z(k) = \sum_{i=1}^{M} p_i(k)\theta_i + \xi(k), \quad k = 1,...,N, \tag{15}$$

where $z(k)$ is the output, $p_i(k)$ are the monomials of the different inputs up to certain degree M, θ_i are the unknown parameters of the model to be estimated, $\xi(k)$ is the modeling error and N is the data length. Equation ,(15) can be transformed to the matrix form

$$Z = P\Theta + \Xi \,. \tag{16}$$

Given this formulation, a linear least squares problem emerges. The proposed OLS method systematically searches the entire regressor space (monomials) as precised in equation (16) to find the best error reduction set, transforms these optimal regressors into orthogonal components, and then perform final regressor identification based on the new orthogonal system. These estimates will be mapped back to the original parameter estimates with their relative regressors given in equations ,(15) and .(16). This is called Parameter Estimation (PE). Structure Selection (SS) algorithm is then applied where it is anticipated that a linear model will emerge. This procedure takes the estimated parameters and statistically prioritizes these regressors into the most significant regressor, second most significant regressor and so on until accuracy of the model output is realized.

The second stage is characterized by the estimation of the model coefficients. A second system identification technique called *recursive least squares* (RLS) is used (Ljung, 1999). This method departs from a system of linear equations in the matrix form

$$Y = P\Theta \,, \tag{17}$$

where $\Theta \in \Re^{M\times 1}$ is the unknown parameters of the model to be determined, $Y \in \Re^{N\times 1}$ is the output vector $P \in \Re^{N\times M}$ is the information matrix which is function of the input and output vectors.

The utility of this method is to calculate the inverse of the information matrix. Based on an algorithm that is composed of three equations, the inverse matrix is simply calculated by means of additions and multiplications. Finally once the inverse of the information matrix is found, the model coefficient vector Θ can be calculated from equation (17).

4.3 Tissue characterization using regular and cylindrical irregular TLM models

A set of inputs were designed. This set was composed of a swept sine, a Schroeder wave, a pulse and a band limited white noise. Swept sine and Schroeder wave signals were the more appropriate candidates since they are characterized by their frequency-rich content and their persistent excitation property. During the model structure identification all the considered inputs except the swept sine gave different model structure of the plaque while its properties were changed. That is why, the swept sine signal was considered to be the best input that captures the dynamics of the studied plaques. The OLS algorithm is applied to the input/output sets of data and a discrete parametric model is established for the plaque. The following simple first order linear model is generated for the different plaques

$$y(k) = a_1 y(k-1) + b_0 u(k) \,, \tag{18}$$

where $y(k)$ is the model output of the plaque and $u(k)$ is the input to the plaque. In order to investigate the effect of plaque acoustic properties variation on the model, a first order continuous model is derived from the input/output data sets

$$\tau\dot{y}(t) + y(t) = du(t) . \quad (19)$$

d is the DC gain and τ the time constant.

The DC gain and the time constant are determined using different approximations of the first derivative of the output, $\dot{y}(t)$. These approximations calculations were performed to test the robustness of the model coefficients when recovering continuous model from discrete model. Multiple first time derivate approximations were performed to recover the continuous model calculations (Centered first order derivative approximation, Forward second order derivative approximation, Backward second order derivative approximation and Centered fourth order derivative approximation). The model coefficients were calculated and compared using these approximations and the error variation was negligible.

The characterization of the plaque will be linked to the model coefficients and mainly the DC gain. The DC gain is expected to decrease if the impedance is increasing. This is explained by the fact that if the acoustic impedance is going up then the density of the plaque is increasing, meaning that this portion of tissue is getting harder and denser mechanically. A denser material has a repulsive effect and the transmitted signal into it is minor. This means that the denser the material is the more resistive effect it shows. Therefore if the impedance goes up then the DC gain is expected to decrease.

In the TLM model, the plaque acoustic impedance is increased gradually and the input/output data sets to this plaque are recorded. The model coefficients (DC gain and pole location) are calculated.

Table 2 illustrates the results of the first order model of the plaque that is obtained from the rectangular TLM model. This model is characterized by a medium that is composed of 90 by 300 nodes in the horizontal and vertical directions respectively and a plaque that is located between the 10^{th} and 30^{th} horizontal nodes and 25^{th} and 65^{th} vertical nodes. The designed swept sine signal is composed of 600 data points with a sampling time that is equal to 10^{-9} sec and a frequency range of $\left[10^4, 10^7\right] Hz$. This input was injected at the 1^{st} horizontal and 45^{th} vertical node. The 45^{th} vertical direction coincides with the middle line crossing the plaque. The input (10^{th} radial position) and output (31^{st} radial position) signals to the plaque were recorded.

Acoustic Impedance $[Kgm^{-2}s^{-1}]$	DC gain d	Time constant τ
$Z_{healthyTissue}$=1559216	0.5634	22.15
$Z=1.2xZ_{healthyTissue}$	0.5171	21.95
$Z=1.4xZ_{healthyTissue}$	0.4778	21.81
$Z=1.6xZ_{healthyTissue}$	0.4442	21.71
$Z=1.8xZ_{healthyTissue}$	0.4149	21.64
$Z=2xZ_{healthyTissue}$	0.3893	21.61

Table 2. Time constant and DC gain variation as function of the acoustic impedance of the plaque (rectangular TLM model)

Table 2 confirms that the DC gain is indeed decreasing when the acoustic impedance of the plaque in increased. Moreover, the time constant τ (indicator of the time response of the system) is decreasing likewise the DC gain when the acoustic impedance is increased. This is explained physically by the fact that the increase of the hardness of the tissue (the plaque) will affect the speed of the system response. The coefficients percentage variations are summarized in Table 3.

Acoustic Impedance $[Kgm^{-2}s^{-1}]$	Acoustic impedance change [%]	DC gain d	DC gain change [%]	Time Constant τ	Time Constant change [%]
$Z=1.2xZ_{healthyTissue}$	20	0.5171	-8.22	21.95	-0.90
$Z=1.4xZ_{healthyTissue}$	40	0.4778	-15.19	21.81	-1.50
$Z=1.6xZ_{healthyTissue}$	60	0.4442	-21.16	21.71	-1.99
$Z=1.8xZ_{healthyTissue}$	80	0.4149	-26.36	21.64	-2.30
$Z=2xZ_{healthyTissue}$	100	0.3893	-30.90	21.61	-2.44

Table 3. DC gain and Time constant variation in percentage (rectangular TLM model)

Using the cylindrical irregular TLM model, the same plaque size and location as of the regular TLM model is considered. The plaque is located between the 10th and 30th radial nodes and 25th and 65th angular nodes. The same designed swept sine signal is injected at the 1st radial and 45th angular node. The 45th angular direction coincides with the middle line crossing the plaque. The input (10th radial position) and output (31st radial position) signals to the plaque are recorded. To study the plaque type effect on the model coefficients, the variation of the DC gain and pole location is studied as function of the plaque density variation. Therefore the speed is set constant and the density of the plaque is varying with respect the healthy tissue density. The same approximations are used to determine the coefficients of the continuous model. As in the case of the regular TLM model section, it is expected that both the DC gain and the time constant to decrease when the acoustic impedance of the plaque is increased and this is what is presented in Table 4.

Acoustic Impedance $[Kgm^{-2}s^{-1}]$	DC gain d	Time Constant τ
$Z_{healthyTissue}=1559216$	0.5275	26.42
$Z=1.2xZ_{healthyTissue}$	0.5224	25.04
$Z=1.4xZ_{healthyTissue}$	0.5090	23.28
$Z=1.6xZ_{healthyTissue}$	0.4910	21.34
$Z=1.8xZ_{healthyTissue}$	0.4699	19.30
$Z=2xZ_{healthyTissue}$	0.4472	17.28

Table 4. DC gain and Time constant variation as function of the acoustic impedance of the plaque (cylindrical irregular TLM model)

It can be seen from both models that a plaque could be characterized by a first order system. In fact the coefficients variation of this model is inversely proportional to the acoustic impedance variation. The coefficients variations are summarized in Table 5.

Acoustic Impedance $[Kgm^{-2}s^{-1}]$	Acoustic impedance change [%]	DC gain d	DC gain change [%]	Time Constant τ	Time Constant change [%]
$Z=1.2xZ_{healthyTissue}$	20	0.5224	-0.97	25.04	-5.22
$Z=1.4xZ_{healthyTissue}$	40	0.5090	-3.51	23.28	-11.88
$Z=1.6xZ_{healthyTissue}$	60	0.4910	-6.92	21.34	-19.23
$Z=1.8xZ_{healthyTissue}$	80	0.4699	-10.92	19.30	-26.95
$Z=2xZ_{healthyTissue}$	100	0.4472	-15.22	17.28	-34.60

Table 5. DC gain and Time constant variation in percentage (cylindrical irregular TLM model)

Considering the model structure found during the tissue characterization, the plaque can be viewed as *a first order low pass filter*. This first order filter illustrated in Fig. 19 is characterized by a DC gain and a time constant that decrease when the resistance R_1 is increasing.

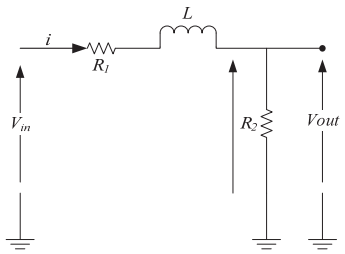

Fig. 19. RL low pass filter

The transfer function of this filter is the following

$$TF = \frac{\frac{R_2}{R_1+R_2}}{1+\frac{L}{R_1+R_2}s}. \tag{16}$$

The resistance R_1 and R_2 can be linked to the acoustic impedance of the medium. From the transfer function above, if R_1 and R_2 increases the DC gain and the time constant decrease.

5. Conclusions

In this paper, ultrasound wave propagation through biological tissues and specifically through arterial wall was studied. This modeling work was twofold. First it departed from a

simple regularly-shaped medium (rectangular geometry) where a transmission line matrix (TLM) model was employed to capture the ultrasound wave propagation. In a second step an irregular TLM model was constructed based on a circular-shaped medium (disk) to simulate IVUS. Both of these models were based on the discretization of the medium where the Huygens principle was applied in the propagation process from one node to another. Moreover the propagating ultrasound waves were recorded in a digitized format in any location at any time specified during the numerical simulation.

Advanced system identification techniques were, then, introduced and applied to characterize tissues. This approach used specific simulated waves in terms of locations to serve as the input/output data sets for the dynamic identification of these regions of interest. This characterization was based upon the construction of parametric models in the form of transfer function where its coefficients are directly related to each plaque type. A first order structure was, thus, found for all plaque types with different DC gain and time constant values depending on the properties of these inclusions.

Finally, a quantitative study was performed to link the variation of these two parameters with respect to acoustic properties. It has been shown consequently that these plaque characteristics were identified quantitatively based on the ultrasound waves using the system identification approach.

6. References

American Heart Association, AHA. (2008). Statistical Update, 2010, Available from: <http://www.americanheart.org/downloadable/heart/1200594755071International%20Cardiovascular%20Disease%20%20Tables.pdf>

American Heart Association, AHA. (2003). Cardiovascular Disease Statistics, 2010, Available from: < http://www.americanheart.org/presenter.jhtml?identifier=4478>

Gaster, A.L.; Skjoldborg, U.S.; Larsen, J.; Lorsholm, L.; Von Birgelen, C.; Jensen, S.;Thayssen, P.; Pederson, K. E. & Haghfelt, T.H. (2003). Continued improvement of clinical outcome and cost effectiveness following intravascular ultrasound guided PCI: insights from a prospective, randomised study. *Heart*, Vol. 89, No. 9, (September 2003), pp. (1043-1049), ISSN 1468-201X

Mueller, C. ;Hodgson, J.Mc. B.;Schindler, C.;Perruchoud, A. P.; Roskamm, H. & Buettner, H. J. (2003). Cost-Effectiveness of Intracoronary Ultrasound for Percutaneous Coronary Interventions. *American Journal of Cardiology*, Vol. 91, No. 2, (January 2003), pp. (143-147), ISSN 0002-9149

Nissen, S.E. & Yock, P. (2001). Intravascular Ultrasound : Novel Pathophysiological Insights and Current Clinical Applications. *Circulation*, Vol. 103, No. 4, (January 2001), pp. (604-616), ISSN 0009-7322

Stary, H. C. (1992). Composition and classification of human atherosclerotic lesions. *Virchows Archiv*, Vol. 421, No. 4, (June 1992), pp. (277-290), ISSN 0945-6317

Stary, H. C.; Chandler, A. B.; Glagov, S.; Guyton, J.R.; Insull, W.Jr.; Rosenfeld, M.E.; Schaffer, S.A.; Schwartz, C.J.; Wagner, W.D. & Wissler, R.W. (1994). A definition of initial, fatty streak, and intermediate lesions of atherosclerosis. A report from the Committee on Vascular Lesions of the Council on Arteriosclerosis, American Heart Association. *Circulation*, Vol. 89, No. 5, (May 1994), pp. (2462-2478), ISSN 0009-7322

Stary, H.C.; Chandler, A.B.; Dinsmore, R.E.; Fuster, V.; Glagov, S.; Insull, W.Jr.; Rosenfeld, M.E.; Schawrtz, C.J.; Wagner, W.D. & Wissler, R.W. (1995). A Definition of Advanced Types of Atherosclerotic Lesions and a Histological Classification of Atherosclerosis : A Report From the Committee on Vascular Lesions of the Council on Arteriosclerosis, American Heart Association. *Circulation*, Vol. 92, No. 5, (September 1995), pp. (1355-1374), ISSN 0009-7322

Urbani, M.P.; Picano, E.; Parenti, G.; Mazzarisi, A.; Fiori, L.; Paterni, M.; Pelosi, G. & Landini, L. (1993). In vivo radiofrequency-based ultrasonic tissue characterization of the atherosclerotic plaque. *Stroke*, Vol. 24, No. 10, (October 1993), pp. (1507-1512), ISSN 00392499

Picano, E.; Landini, L.; Distante, A.; Sarnelli, R.; Benassi, L. & Abbate, A. (1983). Different degrees of atherosclerosis detected by backscattered ultrasound: an in vitro study on fixed human aortic walls. *Journal of Clinical Ultrasound*, Vol. 11, No. 7, (September 1983), pp. (375-379), ISSN 0091-2751

Sarnelli, R.; Landini, L. & Squartini F. (1986). Atherosclerosis detection by ultrasounds. A comparative histologic study on aortic specimens. *Applied Pathology*, Vol. 4, No. 4, (1986), pp. (270-275), ISSN 0252-1172

Landini, L.; Sarnelli, R.; Picano, E. & Salvadori M. (1986). Evaluation of frequency dependence of backscatter coefficient in normal and atherosclerotic aortic walls. *Ultrasound in medicine & biology*, Vol. 12 No. 5, (May 1986), pp. (397-401), ISSN 0301-5629

Barzilai, B.; Saffitz, J.E.;Miller, J.G. & Sobel, B.E. (1991). Quantitative ultrasonic characterization of the nature of atherosclerotic plaques in human aorta. *Circulation Research*, Vol. 60, No. 3, (March 1991), pp. (459-463), ISSN 0009-7330

De Kroon, M.G.M.; Van der Wal, L.F.; Gussenhoven, W.J. & Bom, N. (1991). Angle-dependent backscatter from the arterial wall. *Ultrasound in medicine & biology*, Vol. 17, No. 2, (February 1991), pp. (121-126), ISSN 0301-5629

Picano, E.; Landini, L.; Urbani, M.P.; Mazzarisi, A.; Paterni , M. & Mazzone, A.M. (1994). Ultrasound tissue characterization techniques in evaluating plaque structure. *American Journal of Cardiac Imaging*, Vol. 8, No. 2, (April 1994), pp. (123-128), ISSN 0887-7971

Cespedes, E. I.; Ponnekanti, H.; Yazdi, Y. & Li, X. (1991). Elastography: a quantitative method for imaging the elasticity of biological tissues. *Ultrasonic Imaging*, Vol. 13, No. 2, (April 1991), pp. (111-134), ISSN 0161-7346

Ryan, L.K. & Foster, F.S. (1997). Ultrasonic measurement of differential displacement and strain in vascular model. *Ultrasonic Imaging*, Vol. 19, No. 1, (January 1997), pp. (19-38), ISSN 0161-7346

De Korte, C.L.; Cespedes, E.I.; Van der steen, A.F.; Pasterkamp, G. & Bom, N. (1998). Intravascular ultrasound elastrography: assessment and imaging of elastic properties of diseased arteries and vulnerable plaque. *European Journal of Ultrasound*, Vol. 7, No. 3, (August 1998), pp. (219-224), ISSN 0929-8266

Achaar, J. A.; De Korte, C.L.; Mastik, F.; Strijder, C.; Pasterkamp, G.; Boersma, E.; Seerruys, P.W. & Van Der Steen, A.F. (2003). Characterizing Vulnerable Plaque Features With Intravascular Elastography. *Circulation*, Vol. 108, No. 21, (November 2003), pp. (2636-2641), ISSN 0009-7322

Saijo, Y.; Tanaka, A.; Owada, N.; Akino, Y. & Nitta, S. (2004). Tissue velocity imaging of coronary artery by rotating-type intravascular ultrasound. *Ultrasonics*, Vol. 42, No. 1-9, (April 2004), pp. (753-757), ISSN 0041-624X

Shapo, B.M.; Crowe, J.R.; Erkamp, R.; Emelianov, S.Y.; Eberle, M.J. & O'donnell, M. (1996). Strain imaging of coronary arteries with intraluminal ultrasound: experiments on an inhomogeneous phantom. *Ultrasonic Imaging*, Vol. 18, No. 3, (July 1996), pp. (173-191), ISSN 0161-7346

De Korte, C. L.; Pasterkamp, G.; Van Der Steen, A.F.W.; Woutman, H.A. & Bom, N. (2000). Characterization of Plaque Components With Intravascular Ultrasound Elastography in Human Femoral and Coronary Arteries In Vitro. *Circulation*, Vol. 102, No. 6, (August 2000), pp. (617-623), ISSN 0009-7330

Koenig, A. & Klauss, V. (2007). Virtual Histology. *Heart*, Vol. 93 No. 8, (May 2007), pp. (977-982), ISSN 1468-201X

Nair, A.; Kuban, B.D.; Tuzcu, E.M.; Schoenhagen, P.; Nissen, S.E. & Vince, D.G. (2002). Coronary Plaque Classification With Intravascular Ultrasound Radiofrequency Data Analysis. *Circulation*, Vol. 106, No. 18, (May 2002), pp. (2200-2206), ISSN 0009-7330

Kuznestov, V.P. (1971). Equations of nonlinear acoustics. *Soviet Physics - Acoustics*, Vol. 16, (1971), pp. (467-470), ISSN 0038-562X

Lee, Y.S. & Hamilton, M.F. (1995). Time-domain modeling of pulsed finite-amplitude sound beams. *Journal of the Acoustical Society of America*, Vol. 97, No. 2, (February 1995), pp. (906-917), ISSN 0001-4966

Tavakkoli, J.; Cathignol, D. & Souchon, R. (1998). Modeling of pulsed finite-amplitude focused sound beams in time domain. *Journal of the Acoustical Society of America*, Vol. 104, No. 4, (October 1998), pp. (2061-2072), ISSN 0001-4966

Kendall, A. & Weimin, H. (June 2007*). Theoretical Numerical Analysis- A functional analysis framework*, (Second edition), Springer, ISBN 0387258876, New York, USA

Guenther, R.B. & John, W.L. (1996). *Partial differential equations of mathematical physics and integral equation*. Dover publications, ISBN 9780486688893, New York, USA

CliffsNotes.com. *Wave Optics*. 12 Apr 2011 <http://www.cliffsnotes.com/study_guide/topicArticleId-10453,articleId-10442.html>

Christos, C. (1995). *The Transmission-Line Modeling Method TLM*, John Wiley & Sons, ISBN 0780310179, New York, USA

De Cong, D.; O'Connor, W.J. &Pulko, S. (2006). *Transmission Line Matrix in Computational Mechanics*, Taylor & Francis, ISBN 0415327172, Boca Raton, Florida, USA

Al-Mukhtar, D.A. & Sitch, J.E. (1981). Transmission-line matrix method with irregularly graded space. *IEEE Proc*, Vol. 128, No. 6, (December 1981), pp. (299-305), ISSN 0143-7097

Bakshi, U.A. & Bakshi, V.U. (2009). *Basic Electrical Engineering*, Technical Publications Pune, ISBN 8184312571, India

Soderstrom, T. & Stoica, P. (2001). *System Identification*, Prentice Hall, ISBN 0138812365, New York, USA

Ljung, L. (1999). *System identification: theory for the user,* (Second edition), Prentice Hall, ISBN 0136566952, New York, USA

Korenberg, M.; Billings, S.A.; Liu, Y.P. & McIlroy, P.J. (1988). Orthogonal parameter estimation algorithm for non-linear stochastic systems. *International Journal of Control*, Vol. 48, No. 1, (January 1988), pp. (193-210), ISSN 0020-7179

Chen, S.; Billings, S.A. & Luo, W. (1989). Orthogonal least squares methods and their application to non-linear system identification. *International Journal of Control*, Vol. 50, No. 5, (November 1989), pp. (1873 - 1896), ISSN 0020-7179

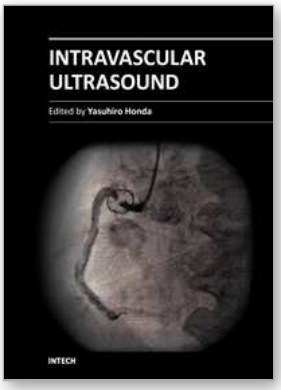

Intravascular Ultrasound
Edited by Dr. Yasuhiro Honda

ISBN 978-953-307-900-4
Hard cover, 207 pages
Publisher InTech
Published online 01, February, 2012
Published in print edition February, 2012

Intravascular ultrasound (IVUS) is a cardiovascular imaging technology using a specially designed catheter with a miniaturized ultrasound probe for the assessment of vascular anatomy with detailed visualization of arterial layers. Over the past two decades, this technology has developed into an indispensable tool for research and clinical practice in cardiovascular medicine, offering the opportunity to gather diagnostic information about the process of atherosclerosis in vivo, and to directly observe the effects of various interventions on the plaque and arterial wall. This book aims to give a comprehensive overview of this rapidly evolving technique from basic principles and instrumentation to research and clinical applications with future perspectives.

INTECH
open science | open minds

InTech Europe
University Campus STeP Ri
Slavka Krautzeka 83/A
51000 Rijeka, Croatia
Phone: +385 (51) 770 447
Fax: +385 (51) 686 166
www.intechopen.com

InTech China
Unit 405, Office Block, Hotel Equatorial Shanghai
No.65, Yan An Road (West), Shanghai, 200040, China
中国上海市延安西路65号上海国际贵都大饭店办公楼405单元
Phone: +86-21-62489820
Fax: +86-21-62489821